tvst

Article

Compartmental Differences in Macular Retinal Ganglion Cell Function

Diego Alba[1], Amy M. Huang[1], Shiva Roghaee[1], Akil Hinds[1], Maja Kostic[1], Tsung-Han Chou[1], and Vittorio Porciatti[1]

[1] Bascom Palmer Eye Institute, University of Miami Miller School of Medicine, Miami, FL, USA

Correspondence: Vittorio Porciatti, Bascom Palmer Eye Institute, University of Miami Miller School of Medicine, 1638 NW 10th Ave., Room 101, Miami, FL 33136, USA.
e-mail: vporciatti@med.miami.edu

Received: December 18, 2020
Accepted: March 2, 2021
Published: March 24, 2021

Keywords: retinal ganglion cell function; pattern electroretinogram; macula

Citation: Alba D, Huang AM, Roghaee S, Hinds A, Kostic M, Chou T-H, Porciatti V. Compartmental differences in macular retinal ganglion cell function. Trans Vis Sci Tech. 2021;10(3):28, https://doi.org/10.1167/tvst.10.3.28

Purpose: The purpose of this study was to investigate local differences of macular retinal ganglion cell (RGC) function by means of the steady-state pattern electroretinogram (SS-PERG).

Methods: SS-PERGs were recorded in healthy subjects ($n = 43$) in response to gratings (1.6 c/deg, 15.63 reversals/s, and 98% contrast) presented on an LED display (800 cd/m^2, 12.5 degrees eccentricity at 30 cm viewing distance) partitioned in triangular sectors (inferior [I]; nasal [N]; superior [S]; and temporal [T]) or concentric regions (central [C] and annulus [A]). For each partition, response amplitude (nV), amplitude adaptation (% change over recording time), phase/latency (deg/ms), and oscillatory potentials (OPs) amplitude (root mean square [RMS] nV) were measured. Data were analyzed with Generalized Estimating Equation (GEE) statistics.

Results: Amplitude differed ($P < 0.001$) between sectors (I: 254 nV; N: 328 nV; S: 275 nV; T: 264 nV; and N>T, I) as well as concentrically (C: 684 nV; A: 323 nV; and C>A). Latency did not differ between sectors (range = 53–54 ms, $P = 0.45$) or concentrically (range = 51–51 ms, $P = 0.7$). Adaptation did not differ ($P = 0.66$) concentrically (C: −19% and A: −22%) but differed ($P = 0.004$) between sectors (I: +25% and S: −29%). The OP amplitude did not differ ($P = 0.5$) between sectors (range = 63–73 nV) as well as concentrically (range = 82–90 nV, $P = 0.3$).

Conclusions: Amplitude profiles paralleled RGC densities from histological studies. Adaptation profile suggested greater autoregulatory challenge in the inferior retina. Latency profile may reflect axonal conduction time to the optic nerve head assuming a direct relationship between axon length and its size/velocity. Location-independent OPs may reflect preganglionic activity.

Translational Relevance: Normal macular RGC function displays local differences that may be related to local vulnerability in optic nerve disorders.

Introduction

The spatial distribution of retinal ganglion cell (RGC) density in the primate central retina is highly nonuniform, with densities in the parafovea exceeding those of the perifovea and those in the nasal retina exceeding those in the temporal retina.[1–4] Nonuniformity of spatial RGC density is reflected in the profile of the ganglion cell inner plexiform layer (GCIPL) thickness, as determined by frequency-domain optical coherence tomography (FD-OCT).[5,6] Several studies have used variants of the pattern electroretinogram (PERG), a sensitive measure of RGC function,[7–9] to investigate local responses in healthy and diseased central retina.[10–21] It is still not well-established whether the magnitude of the PERG signal reflects the magnitude of RGC density at multiple locations, whether PERG latency reflects the conduction time of intraretinal axons, and whether local PERGs have unique features that may provide clues on regional RGC vulnerability in optic nerve disease, such as glaucoma and optic neuritis.

Here, we use the steady-state pattern electroretinogram (SS-PERG) in healthy subjects to noninvasively record responses from partitions of the macular region,

Copyright 2021 The Authors

This work is licensed under a Creative Commons Attribution-NonCommercial-NoDerivatives 4.0 International License.

using a recently developed method that takes advantage of light-emitting diode (LED) displays with high luminance and high temporal resolution[22,23] to generate response with high signal-to-noise ratio (SNR). Analysis of local SS-PERGs will include assessment of response amplitude, amplitude temporal dynamics (adaptation), latency, and oscillatory potentials (OPs), which represent different functional aspects of RGCs and inner retinal neurons impinging on them. PERG amplitude primarily reflects the function of healthy RGCs.[24] SS-PERG amplitude adaptation during continued stimulus presentation reflects the ability of RGCs to regulate their electrical activity in association to increased metabolic demand.[22,25,26] SS-PERG adaptation is reduced in glaucoma[27] and optic neuritis,[28,29] and it is abolished in nonarteritic ischemic optic neuropathy (NAION).[23] SS-PERG latency includes a delay of RGC response in its processing of the pattern stimulus[12] as well as RGC axon activity and conduction time.[30] SS-PERG latency may be delayed in glaucoma[31] and shortened in optic neuritis.[29,32] ERG OPs are thought to originate from preganglionic inner retina circuitry[33,34] and are also measurable in the PERG.[18,35]

Results show that there are differences in the SS-PERG signal between different compartments of the macular region, suggesting that local RGC function reflects both the density and specific properties of RGCs.

Methods

Subjects

We tested a mixed population of healthy subjects (N = 43, 86 eyes, mean age = 31.62 ± 9.48 years; best corrected Snellen visual acuity ≥20/20) with no history of ophthalmological, neurological, or systemic diseases. The study followed the tenets of the Declaration of Helsinki and was approved by the Institutional Review Board of the University of Miami. Informed written consent was obtained from all subjects after the nature of the test and possible risks were explained in detail.

PERG Method

The SS-PERG was recorded using a commercial device (Jorvec Corp., Miami, FL). As previously described,[23] the visual stimulus consisted of a black-white horizontal grating (1.6 cycles/deg, 15.63 reversals/s, 98% contrast, and 800 cd/sqm mean luminance) generated on an LED tablet (14 × 14 cm) and presented binocularly at 30 cm viewing distance in a dimly lit room. With the fast LED display we used, the pattern reversal occurs rapidly and simultaneously over the entire field, whereas with conventional cathode ray tube (CRT) or liquid crystal display (LCD) displays the pattern reversal is completed in a slow sweeping manner over the stimulus field, which would be unsuitable to investigate sectoral latency changes.[36] Subjects wore corrective lenses as needed for the viewing distance. The SS-PERG was recorded simultaneously from both eyes by means of skin electrodes taped on the lower eyelids and referenced to the ipsilateral temples. SS-PERG signals were amplified (100,000 times), filtered (1–300 Hz), and averaged over 1024 epochs (16 consecutive samples of 64 epochs each) in sync with the contrast reversal, automatically rejecting epochs occasionally contaminated by blink artifacts (recording time ~ 2.18 minutes). The recording system automatically calculated the amplitude difference between the first 256 epochs (samples 1–4) and the last 256 epochs (samples 13–16) to assess the time-dependent amplitude change (defined as "PERG adaptation").[22,23] The system also automatically calculated the response noise as the difference between even and odd epochs over the entire recording time.[23]

PERG Waveform Analysis

At the reversal rate of 15.63 reversals/s, PERG waveforms generated by each contrast reversals merge, resulting in a sinusoidal-like waveform (SS-PERG) whose first positive peak corresponds to the P50 wave of the standard transient PERG and the negative trough is dominated by the N95 wave of the standard transient PERG.[36,37] The SS-PERG waveforms were automatically submitted to Fourier analysis to isolate the harmonic component at the reversal frequency (15.63 Hz) and measure its zero-to-peak amplitude in nanovolts (defined as "PERG amplitude") and phase (degrees). As previously described,[23,32] phase values were converted in latency in milliseconds (defined as "PERG latency") considering that one reversal period (360 degrees) corresponded to 1/15.63 Hz = 0.064 second. The formula for calculating PERG latency from PERG phase was (latency [ms] = [360 – phase]/360 * 64). PERG latencies converted from phase coincided with the time-to-peak of the first positive wave of the SS-PERG (Fig. 1). The SS-PERG waveform also included a series of superimposed wavelets (defined as "PERG oscillatory potentials" [OPs]) that were isolated with high-pass filtering (65–300 Hz) and measured as root mean square (RMS) voltage in nanovolts. The OP noise was calculated by averaging in counterphase the OP waveforms

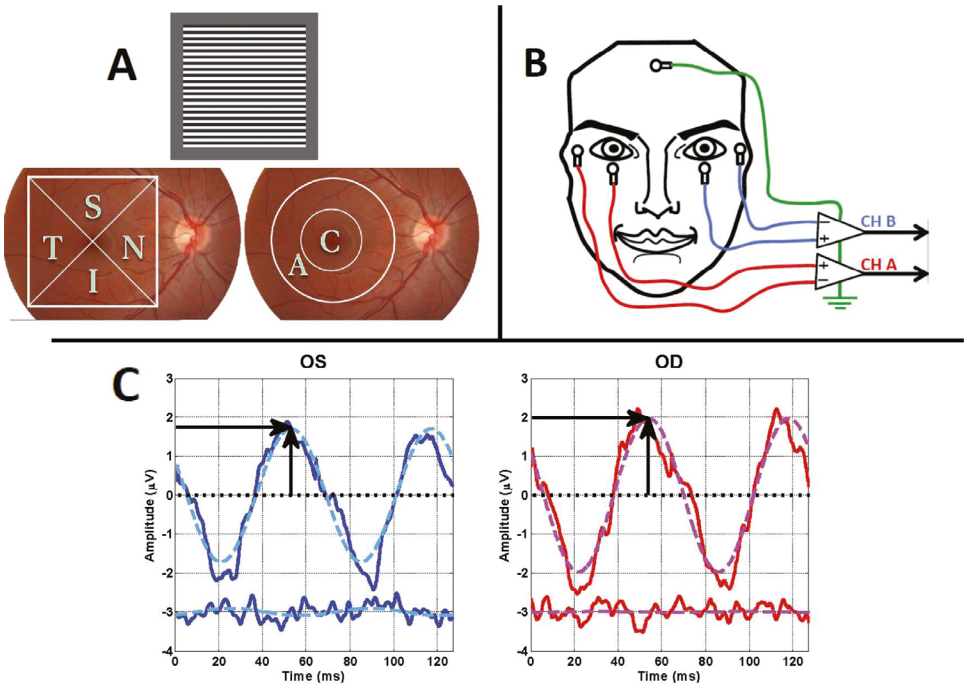

Figure 1. Experimental set up. (**A**) Partition of the pattern stimulus in either radial sectors (inferior [I]; nasal [N]; superior [S]; and temporal [T]) or concentric sectors (center [C] and annulus [A]). (**B**) Electrode montage for PERG recording (active, lower eyelid; reference, ipsilateral temple; common ground, and central forehead). (**C**) Examples of SS-PERG and noise waveforms (thick lines) recorded simultaneously from both eyes in response to full field pattern stimulus (two reversal periods are shown). The smooth dashed lines superimposed to the thick lines represent the actual Fourier-isolated component that has been measured (vertical arrow, zero-to-peak amplitude; horizontal arrow, and time-to-peak latency). Modified from Monsalve et al. 2017.

of the first and second half of the stimulus period (two reversals), resulting in OP cancellation and isolation of residual OP noise.

Stimulus Partition

For the purpose of this study, the visual display was partitioned radially in 4 triangular sectors with the vertex in the fovea (right, left, upper, and lower) of equal area (156 deg^2) spanning 12.5 degrees eccentricity from the fovea. Sectors were presented one at a time, the remaining sectors were covered with an opaque grey cardboard. SS-PERG responses were expressed in terms of the retinal region they were originating from (inferior [I]; nasal [N]; superior [S], and temporal [T]). In a subset of experiments, the visual display was partitioned concentrically in a center (spanning 0–6.2 degrees eccentricity) and an annulus (spanning 6.3–12.5 degrees eccentricity) of an equal area (245 deg^2).

Statistics

Comparisons between PERG originating from different retinal areas were performed using the generalized estimating equation (GEE) method (IBM SPSS statistics version 26). GEE is an unbiased nonparametric method to analyze correlated repeated measures including correlation between the two eyes.

Results

Grand-average SS-PERG and noise waveforms for different retinal partitions are displayed in Figure 2. In both Figure 2 panels A and B, it can be noted that SS-PERGs had consistent waveforms in all partitions, which included OPs on the rising part of the positive wave that could be isolated and analyzed separately. In both Figure 2 panels A and B, it is also apparent that the PERG amplitude was not uniform across partitions, being larger in the nasal sector compared with other sectors and larger in the center compared to the annulus.

Sectoral Compartments Paradigm

Mean SS-PERG amplitudes for sectoral compartments PERG amplitudes ranged between 254 nV

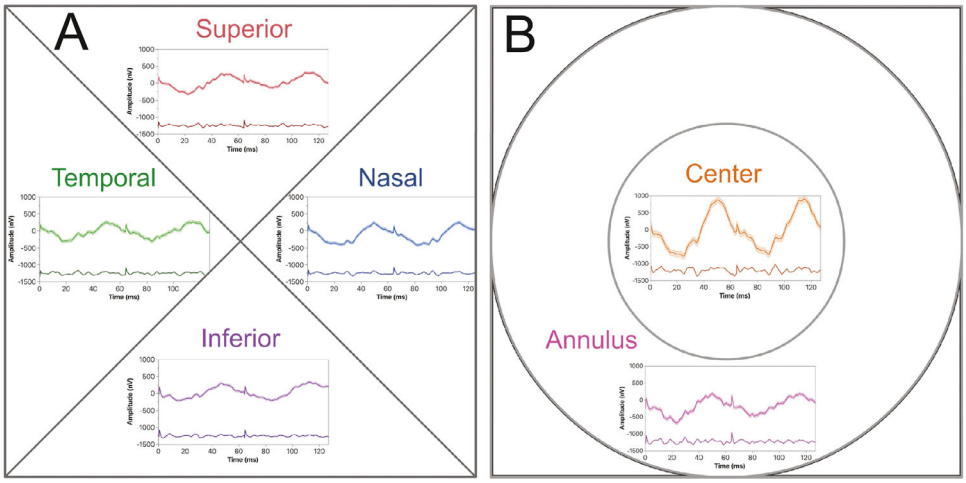

Figure 2. Grand-average SS-PERG waveforms and isolated oscillatory potentials for different radial sectors (**A**) and concentric sectors (**B**). Thin lines superimposed on the thicker PERG waveforms represent ± 1 SEM.

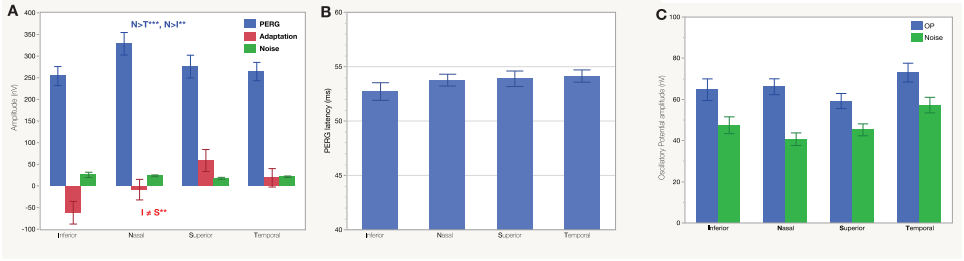

Figure 3. Mean SS-PERG outcome measures for sectoral stimulus compartments. (**A**) Mean amplitude, amplitude adaptation and noise. (**B**) Mean latency. (**C**) Mean oscillatory potentials amplitude and noise. In all panels, error bars represent ± 1 SEM.

and 328 nV, whereas the mean noise amplitudes ranged between 21 and 26 nV. The mean SNR ranged between 13 and 15. Statistical analysis (GEE) showed that although noise amplitude was not significantly different between sectors ($P = 0.7$), there was a highly significant difference in mean SS-PERG amplitude between sectors ($P < 0.001$). The mean SS-PERG amplitude of the nasal sector (328 nV) was significantly higher than that of the temporal sector (264 nV, $P = 0.001$) and that of the inferior sector (254 nV, $P = 0.005$) but not superior (275 nV, $P = 0.15$). SS-PERG amplitude adaptation was also significantly different between sectors (GEE, $P = 0.003$), the inferior sector and superior sectors having adaptation of different signs (inferior: increased by 61 nV, $P = 0.021$; and superior: decreased by 59 nV, $P = 0.024$). Significant sectoral differences of SS-PERG adaptation did not change by including mean amplitude as covariate. Mean SS-PERG latencies (Fig. 3B) obtained by averaging measures of individual subjects ranged between 52.7 ms in the inferior sector and 54.1 ms in the temporal sector and did not significantly differ between sectors (GEE, $P = 0.26$). Mean RMS amplitudes of SS-PERG OPs (Fig. 3C) obtained by averaging measures of individual subjects ranged between 63 nV and 73 nV and did not significantly differ between sectors (GEE, $P = 0.5$). In all sectors, the mean OP amplitude was significantly ($P < 0.0001$) higher than the corresponding OP noise, with a mean SNR of 1.4.

Concentric Compartments Paradigm

Differences in mean SS-PERG amplitude (Fig. 4A) were prominent between the center (684 nV) and the surround (323 nV), GEE statistics, $P < 0.001$. The mean SS-PERG amplitude adaptation was higher in the center (decreased by 146 nV, $P < 0.0001$) compared to the surround (decreased by 87 nV, $P = 0.009$), but the difference was not significant after including mean SS-PERG amplitude as covariate (GEE, $P = 0.36$). The mean noise amplitude was not significantly different (GEE, $P = 0.25$) between the center (36 nV) and the surround (27 nV). The SS-PERG latency (Fig. 4B) was similar in the center (51.0 ms) and in the surround (51.4 ms), GEE, $P = 0.69$. The RMS amplitude of OPs

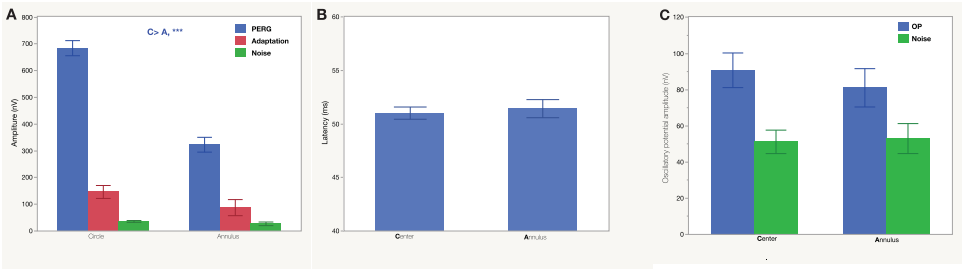

Figure 4. Mean SS-PERG outcome measures for concentric stimulus compartments. (**A**) Mean amplitude, amplitude adaptation and noise. (**B**) Mean latency. (**C**) Mean oscillatory potentials amplitude and noise. In all panels, error bars represent ± 1 SEM.

ranged between 82 nV (center) and 90 nV (surround) and was not significantly different between the two compartments (GEE, $P = 0.3$). In both compartments, the mean OP amplitude was significantly ($P < 0.0001$) higher than the corresponding OP noise, with a mean SNR of 1.6.

Discussion

The present results showed that SS-PERGs in response to an LED generated pattern stimulus could be recorded by means of skin electrodes from individual macular compartments with high (>12) SNR. There were clear differences in the magnitude of the SS-PERG signal between macular compartments of equal area, in broad agreement with previous PERG reports using local stimuli.[10,12,13,15,38,39]

With the sectoral compartment paradigm, the SS-PERG response from the nasal sector had an amplitude larger than that of the temporal (1.24 times) and inferior (1.29 times) sectors. This was in good agreement with histological RGC density data derived from Curcio and Allen, 1990,[3] and in fair agreement with GCIPL thickness data derived from different OCT imaging sources.[5,6]

The SS-PERG adaptation had opposite sign in superior (-25%) and inferior (+29%) sectors. The SS-PERG adaptation in the superior sector was in the range of that reported in normal subjects for full field stimuli,[22,25] whereas inverted SS-PERG adaptation in the inferior sector was similar to that reported in some cases of glaucoma.[26] Inverted SS-PERG adaptation has been interpreted as a negative balance between energy demand and supply at stimulus onset that is later restored by the stimulus-driven increase of blood flow.[26] Interestingly, local blood flow is reported to be lower in the inferior retina compared to the superior retina.[40,41]

SS-PERG latency was not significantly different between sectors. The physiology of PERG latency is not well understood, in part for the technical limitations of standard raster displays that do not allow synchronous pattern reversal over the whole stimulus field. This limitation has been overcome with the synchronous LED display used in the present study. One attractive model is that the PERG signal, even though it is initiated and contributed locally, is generated in part remotely at the level of the optic nerve head (ONH), where axons converge in a bundle producing a strong electrical dipole.[13,42] Thus, if the delay of the ONH-generated SS-PERG signal includes the axonal conduction time, then one would expect a longer latency for the temporal SS-PERG compared to the nasal SS-PERG,[13,43] as RGC axons originating in the temporal sector have a longer trajectory to the ONH compared with RGC axons originating in the nasal sector.[44] The present results show instead that SS-PERG latencies in the nasal and temporal sector are identical. This, however, is not necessarily in conflict with the ONH component model, as axon bundles include fibers of different size/velocity whose composition is location-dependent.[45,46] Nerve fiber bundles in the macular sector, compared with those of the temporal sector, include a higher proportion of smaller/slower axons, and this difference in size/velocity may compensate for the nasal-temporal differences in length of axon trajectories, eventually resulting in similar nasal/temporal SS-PERG latencies. Multifocal PERG studies also show that the time-to-peak of the P1 and N2 waves do not depend on the distance of the stimulated area from the ONH, but rather on the spatial frequency of local stimuli (coarser patterns: shorter latency; and finer patterns: longer latency).[17] Similar spatial frequency dependent changes of SS-PERG latency occur with full field pattern stimuli,[47] and are thought to reflect the relative contribution of activated subpopulations of RGCs with different receptive field size. SS-PERG latency shortening for full field stimuli of fixed spatial frequency occurs in

pathological conditions, such as optic neuritis,[29,32] where small/slow fibers of the papillo-macular bundle are primarily affected,[48] and the residual response is subserved by surviving RGCs whose axons have larger/faster fibers.[32]

OPs are not typically measurable in the standard transient PERG due to the low-pass filtering effect of raster displays used to present the pattern stimulus.[18] Korth (1981)[35] using high-luminance, high-temporal resolution, 25 degrees diameter visual stimulus in Maxwellian view, demonstrated that the transient PERG includes conspicuous OPs. Korth noted that the amplitude of PERG OPs as a function of spatial frequency was band-pass tuned, suggesting that OPs are at least in part generated by lateral inhibitory action of elements with center-surround organization of their receptive field. The present results showed that OPs were recordable from sectoral SS-PERGs. That the amplitude of OPs was similar in all sectors whereas the SS-PERG amplitude was location-dependent may mean that the generator sources of OPs are at least in part different from those of the SS-PERG.

With the concentric compartment paradigm, the SS-PERG response from the center had an amplitude much larger (2.12 times) than that from the annulus. This was in good agreement with the average parafovea/perifovea RGC density ratio (2.6 times) derived from histological data of Curcio and Allen, 1990, in human retinae.[3] The SS-PERG center/annulus amplitude ratio was also in reasonable agreement with the average parafovea/perifovea GCIPL thickness ratio (1.7 times) derived from OCT measurements (wide-angle, swept-source, and 1 mm^2 grid) in healthy subjects.[5,6] The magnitude of SS-PERG adaptation was not significantly different between the center (21%) and the annulus (27%) and was in the range of that reported for full-field pattern stimuli of the same spatial frequency.[22,23] The SS-PERG latency (51 ms) was identical in the center and the annulus and was similar to that reported for full-field pattern stimulus.[23,32] In addition, there were no significant eccentricity-dependent differences in OPs. Altogether, results obtained with the concentric stimulus paradigm showed that the magnitude of the SS-PERG signal primarily reflects the eccentricity-dependent distribution of RGC density, in agreement with previous studies on healthy human subjects.[10–13]

In conclusion, there were sizeable compartmental differences in macular SS-PERG. The center-annulus gradient and the sectoral profile of SS-PERG amplitude were in good agreement with corresponding differences in histological RGC density and OCT-determined GCIPL thickness, further supporting an RGC origin for the SS-PERG. The magnitude of regional SS-PERG adaptation did not correspond to structural and SS-PERG amplitude measurements and helped identifying the inferior sector as a location with peculiar autoregulatory dynamics compared with the other macular compartments. The inferior retina, compared to the superior retina, has been shown to have relatively reduced blood flow and be relatively more vulnerable in glaucoma. SS-PERG latency was similar in the nasal and temporal sector. This is consistent with the model that PERG latency includes an ONH component reflecting the conduction time of RGC axons, whose size and velocity increase with increasing distance between the stimulated sector and the ONH. The magnitude of SS-PERG OPs was not related to SS-PERG amplitude and was location-independent. The present results cannot establish whether SS-PERG OPs are generated by RGCs and their axons or by the preganglionic inner retina. Altogether, recording robust local SS-PERG in the central retinal is feasible using skin electrodes and commercially available instruments, and may provide useful insight on local RGC function in optic nerve disease.

Acknowledgments

Funded by the National Institutes of Health (NIH)-NEI RO1 EY014957, NIH center grant P30-EY014801, unrestricted grant to Bascom Palmer Eye Institute from Research to Prevent Blindness, Inc.

Disclosure: **D. Alba**, None; **A.M. Huang**, None; **S. Roghaee**, None; **A. Hinds**, None; **M. Kostic**, None; **T.-H. Chou**, None; **V. Porciatti**, None

References

1. Perry VH, Cowey A. The ganglion cell and cone distributions in the monkey's retina: implications for central magnification factors. *Vision Res*. 1985;25:1795–1810.
2. Wassle H, Grunert U, Rohrenbeck J, Boycott BB. Cortical magnification factor and the ganglion cell density of the primate retina. *Nature*. 1989;341:643–646.
3. Curcio CA, Allen KA. Topography of ganglion cells in human retina. *J Comp Neurol*. 1990;300:5–25.

4. Silveira LC, Perry VH. The topography of magnocellular projecting ganglion cells (M-ganglion cells) in the primate retina. *Neuroscience*. 1991;40:217–237.
5. Jung JH, Seo JH, Kang MS, Shin J. Comparison of glaucoma diagnostic ability of ganglion cell-inner plexiform layer according to the range around the fovea. *BMC Ophthalmol*. 2019;19:270.
6. Mwanza JC, Oakley JD, Budenz DL, Chang RT, Knight OJ, Feuer WJ. Macular ganglion cell-inner plexiform layer: automated detection and thickness reproducibility with spectral domain-optical coherence tomography in glaucoma. *Invest Ophthalmol Vis Sci*. 2011;52:8323–8329.
7. Baker CL, Jr., Hess RR, Olsen BT, Zrenner E. Current source density analysis of linear and nonlinear components of the primate electroretinogram. *J Physiol*. 1988;407:155–176.
8. Porciatti V. Electrophysiological assessment of retinal ganglion cell function. *Exp Eye Res*. 2015;141:164–170.
9. Luo X, Frishman LJ. Retinal pathway origins of the pattern electroretinogram (PERG). *Invest Ophthalmol Vis Sci*. 2011;52:8571–8584.
10. Hess RF, Baker CL, Jr. Human pattern-evoked electroretinogram. *J Neurophysiol*. 1984;51:939–951.
11. Thompson DA, Drasdo N. Computation of the luminance and pattern components of the bar pattern electroretinogram. *Doc Ophthalmol*. 1987;66:233–244.
12. Porciatti V, Ventura LM. Physiologic significance of steady-state pattern electroretinogram losses in glaucoma: clues from simulation of abnormalities in normal subjects. *J Glaucoma*. 2009;18:535–542.
13. Sutter EE, Bearse MA, Jr. The optic nerve head component of the human ERG. *Vision Res*. 1999;39:419–436.
14. Graham SL, Wong VA, Drance SM, Mikelberg FS. Pattern electroretinograms from hemifields in normal subjects and patients with glaucoma. *Invest Ophthalmol Vis Sci*. 1994;35:3347–3356.
15. Porrello G, Falsini B. Retinal ganglion cell dysfunction in humans following post-geniculate lesions: specific spatio-temporal losses revealed by pattern ERG. *Vision Res*. 1999;39:1739–1745.
16. Salgarello T, Giudiceandrea A, Calandriello L, et al. Pattern electroretinogram detects localized glaucoma defects. *Transl Vis Sci Technol*. 2018;7:6.
17. Bach M, Cuno AK, Hoffmann MB. Retinal conduction speed analysis reveals different origins of the P50 and N95 components of the (multifocal) pattern electroretinogram. *Exp Eye Res*. 2018;169:48–53.
18. Patangay S, Derafshi Z, Vajaranant TS, et al. Three dimensional stimulus source for pattern electroretinography in mid- and far-peripheral retina. *Transl Vis Sci Technol*. 2018;7:8.
19. Kreuz AC, de Moraes CG, Hatanaka M, Oyamada MK, Monteiro MLR. Macular and multifocal PERG and FD-OCT in preperimetric and hemifield loss glaucoma. *J Glaucoma*. 2018;27:121–132.
20. Harrison WW, Viswanathan S, Malinovsky VE. Multifocal pattern electroretinogram: cellular origins and clinical implications. *Optom Vis Sci*. 2006;83:473–485.
21. Monteiro ML, Hokazono K, Cunha LP, Oyamada MK. Correlation between multifocal pattern electroretinography and Fourier-domain OCT in eyes with temporal hemianopia from chiasmal compression. *Graefes Arch Clin Exp Ophthalmol*. 2013;251:903–915.
22. Monsalve P, Ren S, Triolo G, et al. Steady-state PERG adaptation: a conspicuous component of response variability with clinical significance. *Doc Ophthalmol*. 2018;136:157–164.
23. Monsalve P, Triolo G, Toft-Nielsen J, et al. Next generation PERG method: expanding the response dynamic range and capturing response adaptation. *Transl Vis Sci Technol*. 2017;6:5.
24. Bach M, Brigell MG, Hawlina M, et al. ISCEV standard for clinical pattern electroretinography (PERG): 2012 update. *Doc Ophthalmol*. 2013;126:1–7.
25. Porciatti V, Sorokac N, Buchser W. Habituation of retinal ganglion cell activity in response to steady state pattern visual stimuli in normal subjects. *Invest Ophthalmol Vis Sci*. 2005;46:1296–1302.
26. Porciatti V, Ventura LM. Adaptive changes of inner retina function in response to sustained pattern stimulation. *Vision Res*. 2009;49:505–513.
27. Porciatti V, Bosse B, Parekh PK, Shif OA, Feuer WJ, Ventura LM. Adaptation of the steady-state PERG in early glaucoma. *J Glaucoma*. 2014;23:494–500.
28. Fadda A, Di Renzo A, Martelli F, et al. Reduced habituation of the retinal ganglion cell response to sustained pattern stimulation in multiple sclerosis patients. *Clin Neurophysiol*. 2013;124:1652–1658.
29. Jiang H, Gameiro GR, Hu H, et al. Shortened pattern electroretinogram latency and impaired autoregulatory dynamics to steady-state stimuli in patients with multiple sclerosis. *J Neuroophthalmol*. 2021;41(1):60–68.
30. Viswanathan S, Frishman LJ, Robson JG. The uniform field and pattern ERG in macaques with experimental glaucoma: removal of spiking activity. *Invest Ophthalmol Vis Sci*. 2000;41:2797–2810.

31. Ventura LM, Porciatti V, Ishida K, Feuer WJ, Parrish RK, 2nd. Pattern electroretinogram abnormality and glaucoma. *Ophthalmology*. 2005;112:10–19.
32. Monsalve P, Ren S, Jiang H, et al. Retinal ganglion cell function in recovered optic neuritis: faster is not better. *Clin Neurophysiol*. 2018;129:1813–1818.
33. Wachtmeister L. Spatial characteristics of the oscillatory potentials of the electroretinogram. *Acta Ophthalmol (Copenh)*. 1986;64:681–690.
34. Wachtmeister L. Basic research and clinical aspects of the oscillatory potentials of the electroretinogram. *Doc Ophthalmol*. 1987;66:187–194.
35. Korth M. Human fast retinal potentials and the spatial properties of a visual stimulus. *Vision Res*. 1981;21:627–630.
36. Ozdamar O, Toft-Nielsen J, Bohorquez J, Porciatti V. Relationship between transient and steady-state pattern electroretinograms: theoretical and experimental assessment. *Invest Ophthalmol Vis Sci*. 2014;55:8560–8570.
37. Toft-Nielsen J, Bohorquez J, Ozdamar O. Unwrapping of transient responses from high rate overlapping pattern electroretinograms by deconvolution. *Clin Neurophysiol*. 2014;125:2079–2089.
38. Thompson DA, Drasdo N. The origins of luminance and pattern responses of the pattern electroretinogram. *Int J Psychophysiol*. 1994;16:219–227.
39. Yoshii M, Paarmann A. Hemiretinal stimuli elicit different amplitudes in the pattern electroretinogram. *Doc Ophthalmol*. 1989;72:21–30.
40. Harris A, Ishii Y, Chung HS, et al. Blood flow per unit retinal nerve fibre tissue volume is lower in the human inferior retina. *Br J Ophthalmol*. 2003;87:184–188.
41. Tomita R, Iwase T, Ueno Y, et al. Differences in blood flow between superior and inferior retinal hemispheres. *Invest Ophthalmol Vis Sci*. 2020;61:27.
42. Chou TH, Porciatti V. The bioelectric field of the pattern electroretinogram in the mouse. *Invest Ophthalmol Vis Sci*. 2012;53:8086–8092.
43. Hood DC, Bearse MA, Jr, Sutter EE, Viswanathan S, Frishman LJ. The optic nerve head component of the monkey's (Macaca mulatta) multifocal electroretinogram (mERG). *Vision Res*. 2001;41:2029–2041.
44. Jansonius NM, Nevalainen J, Selig B, et al. A mathematical description of nerve fiber bundle trajectories and their variability in the human retina. *Vision Res*. 2009;49:2157–2163.
45. Ogden TE. Nerve fiber layer of the primate retina: morphometric analysis. *Invest Ophthalmol Vis Sci*. 1984;25:19–29.
46. Ogden TE, Miller RF. Studies of the optic nerve of the rhesus monkey: nerve fiber spectrum and physiological properties. *Vision Res*. 1966;6:485–506.
47. Porciatti V, Burr DC, Morrone MC, Fiorentini A. The effects of aging on the pattern electroretinogram and visual evoked potential in humans. *Vision Res*. 1992;32:1199–1209.
48. Yap TE, Balendra SI, Almonte MT, Cordeiro MF. Retinal correlates of neurological disorders. *Ther Adv Chronic Dis*. 2019;10:2040622319882205.